Nonlinear Analysis: Modelling and Control, 2009, Vol. 14, No. 2, 217–247

Finite Element Analysis of Mixed Convection in a Rectangular Cavity with a Heat-Conducting Horizontal Circular Cylinder

Md. M. Rahman[1], **M. A. Alim**[1], **M. A. H. Mamun**[2]

[1]Department of Mathematics
[2]Department of Mechanical Engineering
Bangladesh University of Engineering and Technology
Dhaka-1000, Bangladesh
mmustafizurrahman@math.buet.ac.bd

Received: 2008-03-26 **Revised:** 2008-10-30 **Published online:** 2009-05-26

Abstract. Combined free and forced convection in a two dimensional rectangular cavity with a uniform heat source applied on the right vertical wall is studied numerically. A circular heat conducting horizontal cylinder is placed somewhere within the cavity. The present study simulates a practical system, such as a conductive material in an inert atmosphere inside a furnace with a constant flow of gas from outside. Importance is placed on the influences of the configurations and physical properties of the cavity. The development mathematical model is governed by the coupled equations of continuity, momentum and energy and is solved by employing Galerkin weighted residual finite element method. In this paper, a finite element formulation for steady-state incompressible conjugate mixed convection and conduction flow is developed. The computations are carried out for wide ranges of the governing parameters, Reynolds number (Re), Richardson number (Ri), Prandtl number (Pr) and some physical parameters. The results indicate that both the heat transfer rate from the heated wall and the dimensionless temperature in the cavity strongly depend on the governing parameters and configurations of the system studied, such as size, location, thermal conductivity of the cylinder and the location of the inflow and outflow opening. Detailed results of the interaction between forced airstreams and the buoyancy-driven flow by the heat source are demonstrated by the distributions of streamlines, isotherms and heat transfer coefficient.

Keywords: heat transfer, finite element method, mixed convection, heat conducting horizontal circular cylinder, rectangular cavity.

Nomenclature

AR	aspect ratio	D	cylinder diameter [m]
C_p	specific heat of the fluid at constant pressure [J/kg K]	g	gravitational acceleration [ms^{-2}]
		Gr	Grashof number
CBC	convective boundary conditions	h	convective heat transfer coefficient

H	height of the cavity [m]	Pr	Prandtl number
k	thermal conductivity of fluid [$\mathrm{Wm^{-1}K^{-1}}$]	Ra	Rayleigh number
		Re	Reynolds number
k_s	thermal conductivity of solid [$\mathrm{Wm^{-1}K^{-1}}$]	Ri	Richardson number
		T	dimensional temperature [K]
K	thermal conductivity ratio of the solid and fluid	u, v	velocity components [$\mathrm{ms^{-1}}$]
		U, V	non-dimensional velocity components
L	width of the cavity [m]		
L_x	distance between y-axis and the cylinder center [m]	$\overline{V}$	cavity volume [$\mathrm{m^3}$]
		w	height of the inflow and outflow openings [m]
L_y	distance between x-axis and the cylinder center [m]		
		x, y	Cartesian coordinates [m]
Nu	average Nusselt number	X, Y	non-dimensional Cartesian coordinates
p	pressure [$\mathrm{Nm^{-2}}$]		
P	non-dimensional pressure		

Greek symbols

α	thermal diffusivity [$\mathrm{m^2s^{-1}}$]	ν	kinematic viscosity of the fluid [$\mathrm{m^2s^{-1}}$]
β	thermal expansion coefficient [$\mathrm{K^{-1}}$]		
θ	non-dimensional temperature	ρ	density of the fluid [$\mathrm{Kg\,m^{-3}}$]

Subscripts

i	inlet state	av	average

1 Introduction

The studies of buoyancy driven flow characteristics in cavities are received considerable attention in recent years due to its extensive applications in the field of engineering, for example cooling of electronic devices, furnaces, lubrication technologies, chemical processing equipment, drying technologies etc. Analysis of above phenomena incorporating a solid heat conducting obstruction extends its usability to various other practical situations. Particularly a conductive material in an inert atmosphere inside a furnace with a constant flow of gas from outside constitutes a practical application for the present simulation. Many authors have recently studied heat transfer in enclosures with partitions, which influence the convection flow phenomenon.

Omri and Nasrallah [1] studied mixed convection in an air-cooled cavity with differentially heated vertical isothermal sidewalls having inlet and exit ports by a control volume finite element method. They investigated two different placement configurations of the inlet and exit ports on the sidewalls. Best configuration was selected analyzing the cooling effectiveness of the cavity, which suggested that injecting air through the cold wall was more effective in heat removal and placing inlet near the bottom and exit near the top produce effective cooling. Later on, Singh and Sharif [2] extended

their works by considering six placement configurations of the inlet and exit ports of a differentially heated rectangular enclosure whereas the previous work was limited to only two different configurations of inlet and exit port. At the same time, a numerical analysis of laminar mixed convection in an open cavity with a heated wall bounded by a horizontally insulated plate was presented by Manca et al. [3], where three heating modes were considered: assisting flow, opposing flow and heating from below. Results were reported for Richardson number from 0.1 to 100, Reynolds numbers from 100 to 1000 and aspect ratio in the range 0.1–1.5. They showed that the maximum temperature values decrease as the Reynolds and the Richardson numbers increase. The effect of the ratio of channel height to the cavity height was found to play a significant role on streamline and isotherm patterns for different heating configurations. The investigation also indicated that opposing forced flow configuration has the highest thermal performance, in terms of both maximum temperature and average Nusselt number. Later, similar problem for the case of assisting forced flow configuration was tested experimentally by Manca et al. [4] and based on the flow visualization results, they pointed out that for $Re = 1000$ there were two nearly distinct fluid motions: a parallel forced flow in the channel and a recirculation flow inside the cavity and for $Re = 100$ the effect of a stronger buoyancy determined a penetration of thermal plume from the heated plate wall into the upper channel. Very recently Manca et al. [5] experimentally analyzed opposing flow in mixed convection in a channel with an open cavity below. Recently Rahman et al. [6] studied numerically the opposing mixed convection in a vented enclosure. They found that with the increase of Reynolds and Richardson numbers the convective heat transfer becomes predominant over the conduction heat transfer and the rate of heat transfer from the heated wall is significantly depended on the position of the inlet port.

However, many authors have studied heat transfer in enclosures with heat-conducting body obstruction, thereby influencing the convective flow phenomenon. Shuja et al. [7] investigated the effect of exit port locations and aspect ratio of the heat generating body on the heat transfer characteristics and irreversibility generation in a square cavity. They found that the overall normalized Nusselt number as well as irreversibility was strongly affected by both of the location of exit port and aspect ratios. Papanicolaou and Jaluria [8] studied mixed convection from an isolated heat sources in a rectangular enclosure. Later on, Papanicolaou and Jaluria [9] performed computations on mixed convection from a localized heat source in a cavity with conducting walls and two openings for application of electronic equipment cooling. Hsu et al. [10] numerically investigated mixed convection in a partially divided rectangular enclosure. They considered the divider as a baffle inside the enclosure with two different orientations and indicated that the average Nusselt number and the dimensionless surface temperature dependent on the locations and height of the baffle. Lee et al. [11] considered the problem of natural convection in a horizontal enclosure with a square body. Natural convection in a horizontal layer of fluid with a periodic array of square cylinder in the interior were conducted by Ha et al. [12], in which they concluded that the transition of the flow from quasi-steady up to unsteady convection depends on the presence of bodies and aspect ratio effect of the cell. However, in the previous literature the body was considered as a rigid wall but internal heat transfer was not calculated. Few numerical studies taking into account heat transfer

in the interior of the body have been conducted over the past couple of decades. One of the systematic numerical investigations of this problem was conducted by House et al. [13], who considered natural convection in a vertical square cavity with heat conducting body, placed on center in order to understand the effect of the heat conducting body on the heat transfer process in the cavity. They showed that for given Ra and Pr an existence of conducting body with thermal conductivity ratio less than unity leads to heat transfer enhancement.

As the first step toward accurate flow solutions using the adaptive meshing technique, this paper develops a finite element formulation suitable for analysis of steady-state conjugate mixed convection and conduction problems. The paper starts from the Navier-Stokes equations together with the energy equations to derive the corresponding finite element model. The computational procedure used in the development of the computer program is described. The finite element equations derived and then the computer program developed are then evaluated by example of mixed convection in a rectangular cavity with heat conducting horizontal circular cylinder.

The objective of the present study is to investigate the effect of a heat conducting solid cylinder, which may increase or decrease the heat transfer on mixed convection in a rectangular vented cavity. Numerical solutions are obtained over a wide range of Richardson number, Reynolds number, Prandtl number and various physical parameters. The dependence of the thermal and flow fields on the sizes, locations and thermal conductivity of the cylinder is studied in detail.

2 Model specification

The physical model considered here is shown in Fig. 1 along with the important geometric parameters. A cartesian co-ordinate system is used with origin at the lower left corner of the computational domain. It consists of rectangular cavities with a heat conducting horizontal circular solid cylinder, whose right wall is subjected to hot with T_h temperature while the other sidewalls are kept adiabatic. The cavity dimensions are defined by height H and width L. The inflow opening located on the left adiabatic vertical wall and the outflow opening on the opposite heated vertical wall is arranged as shown in the schematic figures and may vary in location, placed either at the top or bottom position. The cavity presented in Fig. 1(a) is subjected to an external flow that enters via the bottom of the insulated vertical wall and leaves via the bottom of the opposite heated vertical wall. For reasons of brevity, this case will be referred to as BB configuration from now. When the horizontal cold jet enters into the cavity from the bottom of the insulated wall and leaves from the top of the opposite vertical one is shown in Fig. 1(b), this case will be referred as BT configuration. Similarly, Fig. 1(c) and 1(d) are referred to as TB and TT configurations respectively. For simplicity, the heights of the two openings are set equal to the one-tenth of the enclosure height. It is assumed that the incoming fluid flow through the inlet at a uniform velocity, u_i at the ambient temperature T_i and the outgoing flow is assumed to have zero diffusion flux for all variables i.e. convective boundary conditions (CBC). All solid boundaries are assumed to be rigid no-slip walls.

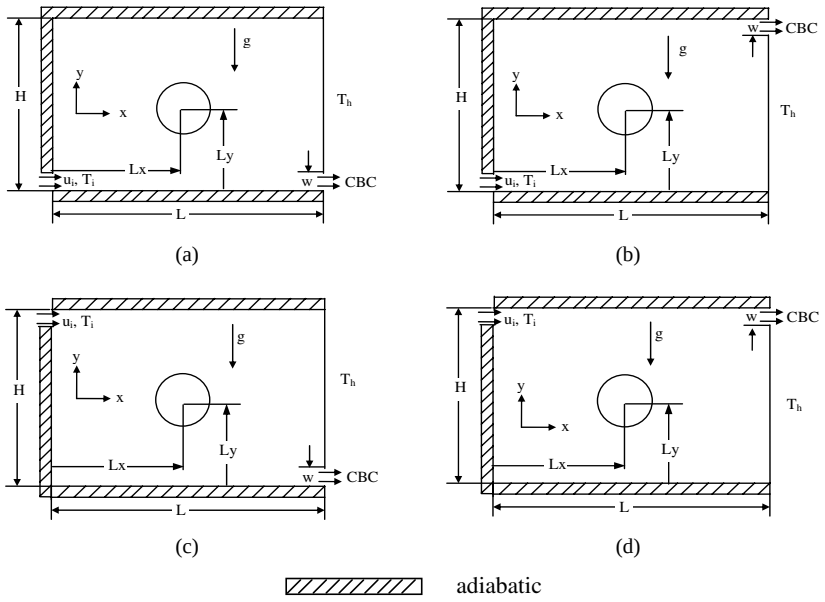

Fig. 1. Four schematic configurations of thermally driven cavity: (a) BB configuration, (b) BT configuration, (c) TB configuration, (d) TT configuration.

3 Mathematical formulation

The flow within the cavity is assumed to be two-dimensional, steady, laminar, incompressible and the fluid properties are to be constant. The radiation effects are taken as negligible and the Boussinesq approximation is used. The dimensionless equations describing the flow are as follows:

$$\frac{\partial U}{\partial X} + \frac{\partial V}{\partial Y} = 0, \tag{1}$$

$$U\frac{\partial U}{\partial X} + V\frac{\partial U}{\partial Y} = -\frac{\partial P}{\partial X} + \frac{1}{Re}\left(\frac{\partial^2 U}{\partial X^2} + \frac{\partial^2 U}{\partial Y^2}\right), \tag{2}$$

$$U\frac{\partial V}{\partial X} + V\frac{\partial V}{\partial Y} = -\frac{\partial P}{\partial Y} + \frac{1}{Re}\left(\frac{\partial^2 V}{\partial X^2} + \frac{\partial^2 V}{\partial Y^2}\right) + Ri\,\theta, \tag{3}$$

$$U\frac{\partial \theta}{\partial X} + V\frac{\partial \theta}{\partial Y} = \frac{1}{RePr}\left(\frac{\partial^2 \theta}{\partial X^2} + \frac{\partial^2 \theta}{\partial Y^2}\right). \tag{4}$$

For solid cylinder the energy equation is

$$0 = \left(\frac{\partial^2 \theta_s}{\partial X^2} + \frac{\partial^2 \theta_s}{\partial Y^2}\right), \tag{5}$$

where $Re = u_i L/v$, $Gr = g\beta\Delta T L^3/v^2$, $Pr = v/\alpha$, $Ri = Gr/Re^2$, and $K = k_s/k$ ($\Delta T = T_h - T_i$ and $\alpha = k/\rho c_p$ are the temperature difference and thermal diffusivity of the fluid respectively) are the Reynolds number, Grashof number, Prandtl number, Richardson number and solid fluid thermal conductivity ratio respectively.

The above equations were non dimensionalized by using the following dimensionless dependent and independent variables

$$X = \frac{x}{L},\ Y = \frac{y}{L},\ U = \frac{u}{u_i},\ V = \frac{v}{u_i},\ P = \frac{p}{\rho u_i^2},\ \theta = \frac{T - T_i}{T_h - T_i},\ \theta_s = \frac{T_s - T_i}{T_h - T_i},$$

where X and Y are the coordinates varying along horizontal and vertical directions respectively, U and V are the velocity components in the X and Y directions respectively, θ is the dimensionless temperature and P is the dimensionless pressure.

Non-dimensional forms of the boundary conditions for the present problem are specified as follows:

At the inlet: $U = 1$, $V = 0$, $\theta = 0$.

At the outlet: convective boundary condition (CBC), $P = 0$.

At all solid boundaries: $U = 0$, $V = 0$.

At the heated right vertical wall: $\theta = 1$.

At the left, top and bottom walls: $\frac{\partial\theta}{\partial N} = 0$.

At the fluid-solid interface: $(\frac{\partial\theta}{\partial N})_{fluid} = K(\frac{\partial\theta_s}{\partial N})_{solid}$.

Where N is the non-dimensional distances either X or Y direction acting normal to the surface and K is the dimensionless ratio of the thermal conductivity (k_s/k).

The average Nusselt number at the heated wall is calculated by $Nu = \frac{1}{L_h}\int_0^{L_h} \frac{h(y)y}{k}\,\mathrm{d}y$ and the bulk average temperature is defined as $\theta_{av} = \int \theta\,\mathrm{d}\overline{V}/\overline{V}$, where L_h and $h(y)$ are the length and the local convection heat transfer coefficient of the heated wall respectively, $\overline{V}$ is the cavity volume and θ_{av} should be minimized.

4 Numerical analysis

The governing equations along with the boundary conditions are solved numerically by employing Galerkin weighted residual finite element techniques. The finite element formulation and computational procedure are discussed detail in Appendix.

4.1 Grid independence test

Geometry studied in this paper is an obstructed vented cavity; therefore several grid size sensitivity tests were conducted in this geometry to determine the sufficiency of the mesh scheme and to ensure that the solutions are grid independent. This is obtained when numerical results of the average Nusselt number Nu, average temperature θ_{av} and solution time become grid size independent, although we continue the refinement of the mesh grid. Five different non-uniform grids with the following number of nodes and elements were considered for the grid refinement tests: 24545 nodes, 3788 elements; 29321 nodes, 4556 elements; 37787 nodes, 5900 elements; 38163 nodes, 5962 elements

and 48030 nodes, 7516 elements as shown in Table 1. From these values, 38163 nodes and 5962 elements can be chosen throughout the simulation to optimize the relation between the accuracy required and the computing time.

Table 1. Grid sensitivity check at $Re = 100$, $Ri = 1.0$, $K = 5.0$, $D = 0.2$ and $Pr = 0.71$

Nodes (elements)	24545 (3788)	29321 (4556)	37787 (5900)	38163 (5962)	48030 (7516)
Nu	4.167817	4.168185	4.168376	4.168394	4.168461
θ_{av}	0.042974	0.042973	0.042973	0.042973	0.042973
Time [s]	323.610	408.859	563.203	588.390	793.125

4.2 Code validation

The present code was extensively validated based on the problem of House et al. [13]. We present here some results obtained by our code in comparison with those reported in House et al. [13] for $Ra = 0.0, 10^5$ and two values of $K = 0.2$ and 5.0. The physical problem studied by House et al. [13] was a vertical square enclosure with sides of length L. The vertical walls were isothermal and differentially heated, where as the bottom and top walls were adiabatic. A square heat conducting body with sides of length equal to $L/2$ was placed at the center of the enclosure. For the same parameters used in House et al. [13]; the average Nusselt number (at the hot wall) comparison is shown in Table 2. The present results have an excellent agreement with the results obtained by House et al. [13].

Table 2. Nusselt number comparison for $Pr = 0.71$

		Nu		
Ra	K	Present work	House et al. [13]	Error (%)
0	0.2	0.7071	0.7063	0.11
0	1.0	1.0000	1.0000	0.00
0	5.0	1.4142	1.4125	0.12
10^5	0.2	4.6237	4.6239	0.00
10^5	1.0	4.5037	4.5061	0.00
10^5	5.0	4.3190	4.3249	0.14

5 Results and discussion

Numerical results have been presented in order to determine the effects of the presence of dimensionless parameters in a rectangular cavity. The dimensionless governing parameters that must be specified for the system are Reynolds number (Re), Richardson number (Ri), Prandtl number (Pr) and the physical parameters in the system are the cylinder diameter (D), solid fluid thermal conductivity ratio (K), location of inlet and outlet

openings of the cavity, location of cylinder in the cavity and cavity aspect ratio (AR). Since so many basic dimensionless parameters are required to characterize a system, a comprehensive analysis of all combinations of these parameters is not practical. The numerical results have been used to explain the effect of several parameters at a small fraction of the possible situations by simplifying the configuration. The presentations of the results have been started with the streamline and isotherm patterns in the cavity. Representative distributions of average Nusselt number at the heated wall and average temperature of the fluid in the cavity have also been presented.

5.1 Effect of inlet and outlet positions

Four different cavity configurations have been investigated for the mixed convection problem in order to compare the behavior of convective heat transfer for different relative inlet and outlet locations. The streamlines corresponding to the four different inlet and outlet positions namely BB, BT, TB and TT with $AR = 1.0$, $Re = 100$, $Ri = 1.0$, $Pr = 0.71$, $L_x = L_y = 0.5$, $D = 0.2$ and $K = 5.0$ have been shown in Figs. 2a(i)–(iv). It has been observed that a large counter-clockwise (CCW) recirculation cell is formed above the main fluid stream for the BB (injection at the bottom of the left insulated wall and exit from the bottom of the heated wall) configuration and it occupies the maximum space of the cavity. This is because the fresh fluid entering the cavity travels the shortest possible distance before leaving the cavity and cannot come into intimate mixing with the hotter fluids. As the outlet port moved along the heated wall at the top corner and keeping the inlet position unchanged, i.e. for BT configuration the CCW recirculation cell reduces in size and is divided into two relatively small vortices, which are located at the left top corner in the cavity. However, for the TB configuration the flow changes its pattern from two recirculation vortices to a single vortex and shifted from left top corner to the right top corner in the cavity. On the other hand, a clock-wise (CW) small eddy is developed near the left insulated wall starting from just below the inlet position whereas the external flow increases its passage region and finally occupies almost the cavity for the TT configuration, which is due to the entering fresh fluids come into intimate mixing with the hotter fluids in the cavity. The contours of the dimensionless temperature (θ) corresponding to the above mentioned four cases with $AR = 1.0$, $Re = 100$, $Ri = 1.0$, $Pr = 0.71$, $L_x = L_y = 0.5$, $D = 0.2$ and $K = 5.0$ have been presented in Figs. 2b(i)–(iv). The value of θ on the heated wall is 1, whereas the value of θ of the fluid entering the cavity is zero and the contour values are incremented by 0.05. From the isotherms shown in Figs. 2b(i)–(iv), it is noticed that the isothermal lines are more uniformly distributed in the cavity for the BB and TB configurations. On the other hand, it has been observed that for TB configuration the high temperature region is more concentrated near the hot wall and the distribution of the isothermal lines is non-uniform in the cavity. It has also been observed that the isothermal lines are more vertically concentrated around the heat source for the TT configuration, which is similar to conduction-like distribution. It is also seen that the thermal boundary layer near the heated wall in the cavity is developed for BT and TT configurations, where as the thermal boundary layer in the cavity is absent for the BB and TB configurations.

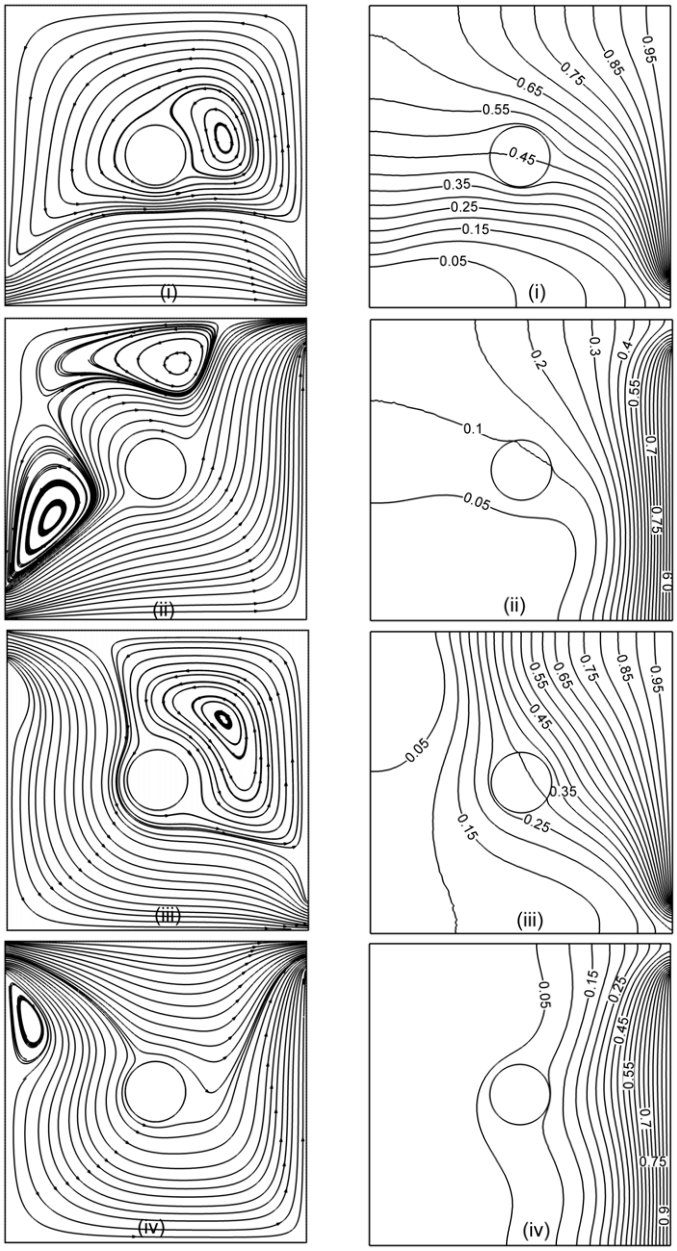

(a) (b)

Fig. 2. (a) Streamlines and (b) isotherms (i) BB, (ii) BT, (iii) TB and (iv) TT configurations while $AR = 1.0$, $Re = 100$, $Ri = 1.0$, $K = 5.0$, $Pr = 0.71$, $L_x = L_y = 0.5$ and $D = 0.2$.

The average Nusselt number (Nu) at the hot wall and the bulk average temperature (θ_{av}) in the cavity have been compared in Fig. 3 for the above four configurations. From this figure it is clear that the Nu is highest for BT configuration. The reason for this is the fresh fluid entering in the bottom of the left wall and travels comparatively long distance and taking heat away from the hot wall before exit the cavity. It can also be seen that the average temperature of the fluid in the cavity is the lowest for the BT configuration in the forced convection dominated region and for the TT configuration in the free convection dominated region.

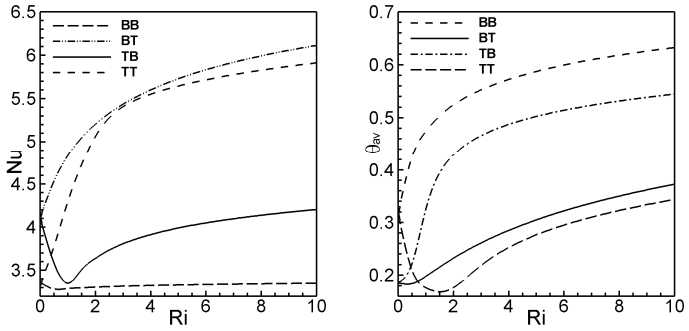

Fig. 3. Effect of inlet and outlet position on average Nusselt number and average temperature while $AR = 1.0$, $Re = 100$, $Pr = 0.71$, $D = 0.2$, $L_x = L_y = 0.5$ and $K = 5.0$.

5.2 Effect of the cylinder diameter

The effects of the heat conducting cylinder on the flow and thermal fields for the BT configuration at $AR = 1.0$, $Re = 100$, $Ri = 1.0$, $Pr = 0.71$, $L_x = L_y = 0.5$ and $K = 5.0$ have been presented in Fig. 4. As compared to Fig. 4a(i), the solid cylinder in the cavity reduces the strength of the recirculation cell induced by the heat source. In Fig. 4a(ii), which is for cylinder of diameter $D = 0.1$, only small differences in the streamlines have been observed when compared with Fig. 4a(i). This is the evidence of no significance influence of a small size solid cylinder on the convective flow of the cavity. On the other hand, as the size of the cylinder increases, the space available for the buoyancy-induced recirculating flow decreases. From the isotherms shown in Figs. 4(i)–(iv), it has been observed that the high-temperature zone is confined to a region close to the hot surface for all cases and the lines are uniformly distributed in the cavity. The last line from the heated wall is the line with $\theta_1 = 0.05$ for all the cases presented in this figure. A closer examination shows that the area between the heated wall and the line $\theta_1 = 0.05$ slightly increase with the increase of the cylinder diameter (D).

Further, in order to evaluate how the presence of the cylinder affects the heat transfer rate along the hot wall, average Nusselt number (Nu) has been plotted as a function of Richardson number (Ri) for four different cylinder diameters ($D = 0$, $D = 0.1$, $D = 0.2$ and $D = 0.4$) shown in Fig. 5.

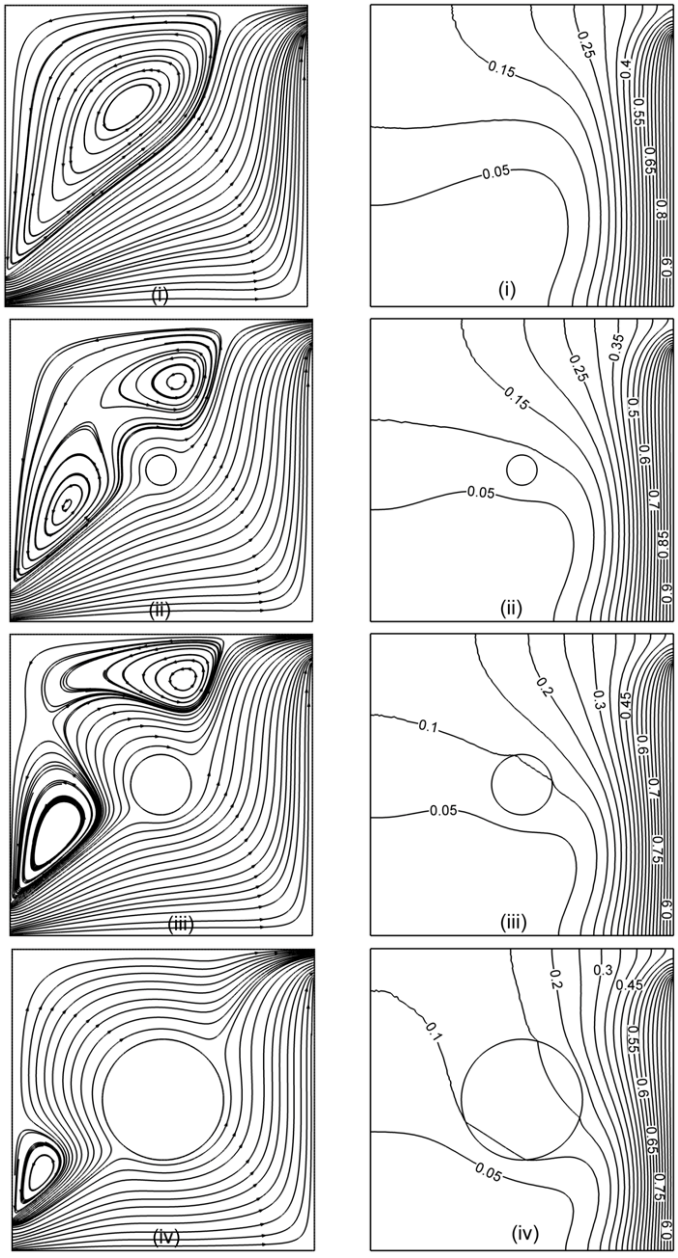

Fig. 4. (a) Streamlines and (b) isotherms for the BT configuration at (i) $D = 0$, (ii) $D = 0.1$, (iii) $D = 0.2$ and (iv) $D = 0.4$ while $AR = 1.0$, $Re = 100$, $Ri = 1.0$, $K = 5.0$, $L_x = L_y = 0.5$ and $Pr = 0.71$.

It has been observed that Nu is the highest for the large cylinder diameter (D = 0.4) at $Ri \leq 6.0$ and beyond this values of Ri the cylinder diameter has insignificant effect on the average Nusselt number at the hot wall. The effect of cylinder diameter on average temperature of the fluid in the cavity is also shown in Fig. 5. From this figure it has been seen that cylinder diameter has little effect on the average temperature (θ_{av}) of the fluid in the cavity. A closer examination of Fig. 5 has revealed that the values of θ_{av} decreases at $Ri \leq 0.5$ and beyond this value of Ri, θ_{av} increases sharply with increasing Ri for all values of D. On the other hand, θ_{av} is the lowest for $D = 0.2$ at $Ri \leq 2.0$ and beyond this value of Ri, θ_{av} is the lowest for $D = 10.0$.

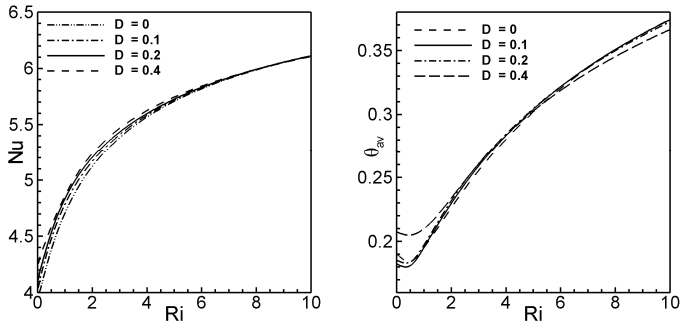

Fig. 5. Effect of cylinder diameter on average Nusselt number and average temperature for the BT configuration while $AR = 1.0$, $Re = 100$, $Pr = 0.71$, $L_x = L_y = 0.5$ and $K = 5.0$.

5.3 Effect of thermal conductivity ratio

The effect of the thermal conductivity ratio of the solid and fluid has also been computed numerically and have shown in Figs. 6 for the BT configuration at $AR = 1.0$, $Re = 100$, $Ri = 1.0$, $Pr = 0.71$, $D = 0.2$ and $L_x = L_y = 0.5$. It has been found that the different heat transfer properties of the cylinder have small effect on the heat transfer in the cavity. The streamlines for these cases appear to be almost identical as shown in the Fig. 6a(i)–(iv). This is because thermal conductivity ratio has no influence on the velocity distribution. The effect of thermal conductivity ratio on the isotherms has been presented in the Figs. 6b(i)–(iv). From these figures it has been seen easily that a concentrated thermal boundary layer near the heated surface has developed for all the cases and the isothermal lines moves away from the centre of the heat conducting cylinder with increasing values of the thermal conductivity ratio.

Average Nusselt number at the hot wall and average temperature of the fluid in the cavity as a function of Richardson number have been shown in Fig. 7 for the BT configuration at $AR = 1.0$, $Re = 100$, $Pr = 0.71$, $L_x = L_y = 0.5$, $D = 0.4$ and $K = 0.2, 1.0, 5.0$ and 10.0. The average Nusselt number at the heated surface is found to be the highest for a relatively low thermal conductivity ratio $K = 0.2$, which is due to the

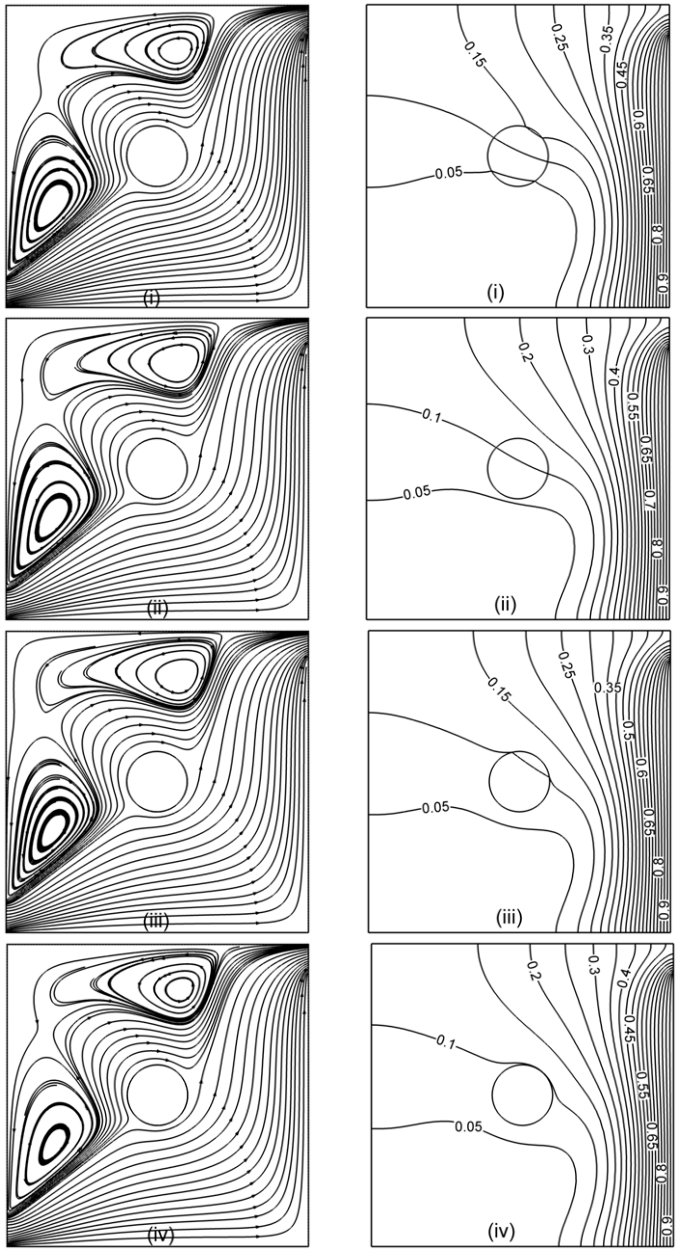

Fig. 6. (a) Streamlines and (b) isotherms for the BT configuration at (i) $K = 0.2$, (ii) $K = 1.0$, (iii) $K = 5.0$ and (iv) $K = 10.0$, while $AR = 1.0$, $Re = 100$, $Ri = 1.0$, $Pr = 0.71$, $L_x = L_y = 0.5$ and $D = 0.2$.

cylinder with low thermal conductivity acts as an insulator and prevents heat transfer between the hot and cold fluid streams. Hence the heat transfer in this case is mainly by mixed convection. The average temperature of the fluid in the cavity decreases for all the cases in the forced convection dominated region and are increases sharply with increasing Ri in the free convection dominated region. On the other hand, the values of θ_{av} is found to be the lowest for $K = 0.2$ at $Ri \leq 2.0$ and beyond this value of Ri, θ_{av} is the lowest for $K = 10.0$.

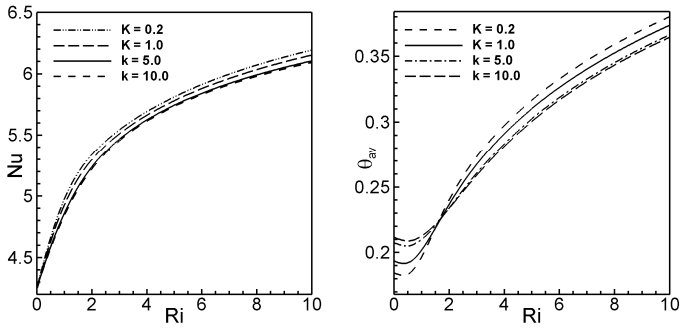

Fig. 7. Effect of thermal conductivity ratio on average Nusselt number and average temperature for the BT configuration while $AR = 1.0$, $Re = 100$, $Pr = 0.71$, $L_x = L_y = 0.5$ and $D = 0.4$.

5.4 Effect of Reynolds number

The effects of the parameter Re on the flow and thermal fields for the BT configuration at $AR = 1.0$, $Ri = 1.0$, $D = 0.2$, $Pr = 0.71$, $L_x = L_y = 0.5$ and $K = 5.0$ have been presented in the Fig. 8. From the Fig. 8a(i) it is found that the open lines of the external flow occupy almost the whole cavity and becomes symmetric about the diagonal from the inlet to the exit for $Re = 50$. Because, of the small value of Re the thermal transport effect by the external cold air is small. At higher $Re = 100$, the pattern of the streamlines become asymmetric shapes about the line from the inlet to the exit. The circulation of the flow shows two rotating vortices near the left top corner of the cavity as shown in Fig. 8a(ii). As the Reynolds number increases up to 150, the role of forced convection in the cavity become more significant, and consequently the circulation in the flow become large with two inner vortices as presented in Fig. 8a(iii). Further increases of the Reynolds number (i.e. $Re = 200$), increases the strength of the recirculation cell, which occupies much portion in the cavity and the two inner vortices become small in size as shown in Fig. 8a(iv). The corresponding temperature distributions have also been seen in Figs. 8b(i)–(iv). From these figures it has been observed that increase in Re reduces the thermal boundary layer thickness near the heated surface and it is possible, since at larger value of Re, the effect of gravitational force become negligible and the flow is governed by the forced convection. The average Nusselt numbers at the heat source and the average temperature in the cavity have been plotted as a function of Richardson number for a

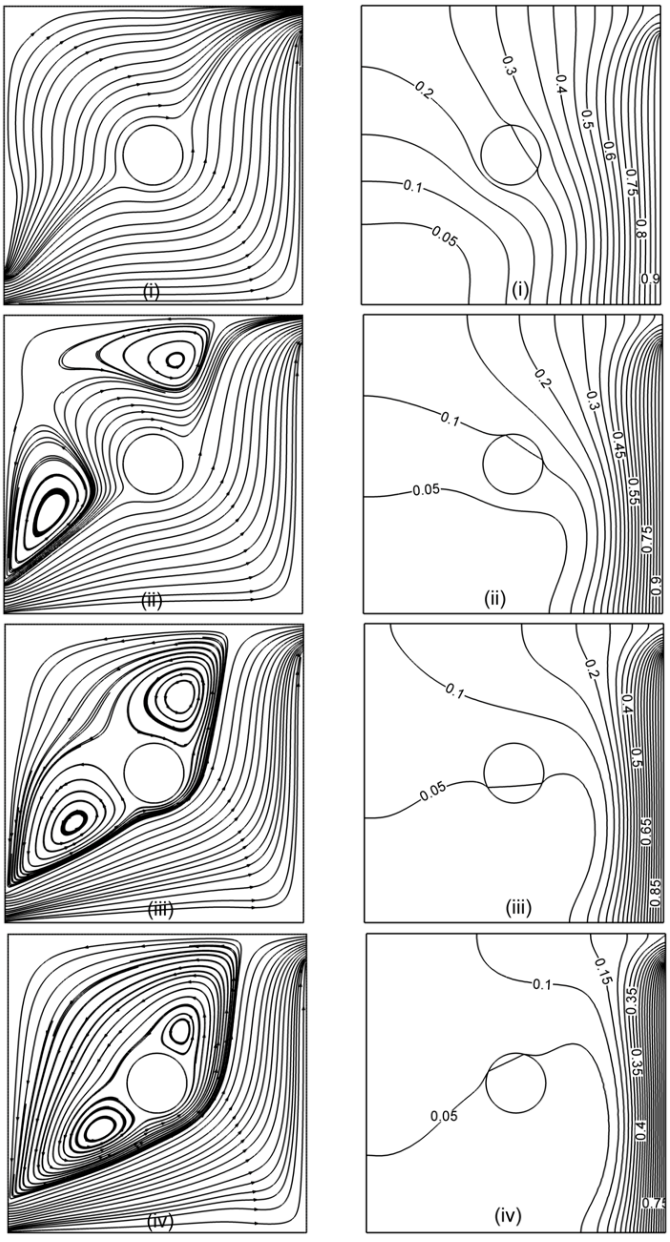

(a) (b)

Fig. 8. (a) Streamlines and (b) isotherms for the BT configuration at (i) $Re = 50$, (ii) $Re = 100$, (iii) $Re = 150$ and (iv) $Re = 200$ while $AR = 1.0$, $Ri = 1.0$, $K = 5.0$, $D = 0.2$, $L_x = L_y = 0.5$ and $Pr = 0.71$.

particular Reynolds numbers (shown in Fig. 9). From this figure it has been observed that for a fixed values of Ri, the average Nusselt number at the hot wall is the highest and average temperature of the fluid in the cavity is the lowest for large values of $Re = 200$. This is due to more heat has been carried away from the heat source and dissipated through the out flow opening for the large values of Re.

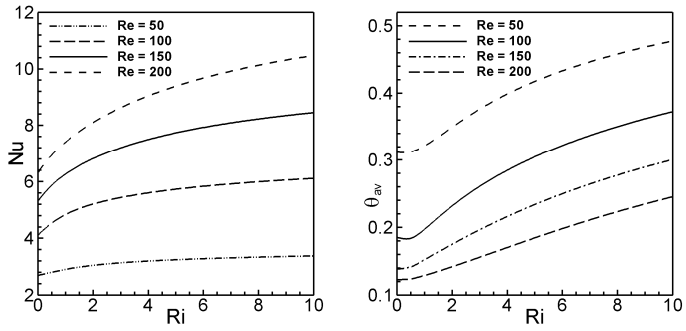

Fig. 9. Effect of Reynolds number on average Nusselt number and average temperature for the BT configuration while $AR = 1.0$, $Pr = 0.71$, $D = 0.2$, $L_x = L_y = 0.5$ and $K = 5.0$.

5.5 Effect of Richardson number

Fig. 10 has been indicated the dynamic and thermal field for the BT configuration at $AR = 1.0$, $Re = 100$, $D = 0.2$, $L_x = L_y = 0.5$, $K = 5.0$ and different Ri in terms of the streamlines and isotherms. The streamlines shown in Fig. 10a(i)–(iv) describe the interaction of forced and natural convection under various convection regimes. For $Ri = 0.0$, the major incoming flow is symmetric about the diagonal joining from the inlet to the exit port and a small vortex is developed near the left insulated wall starting from just above the inlet port, due to the domination of forced convection as shown in Fig. 10a(i). At $Ri = 2.5$, the size of the vortex is increased dramatically and changes its pattern from a uni-cellular vortex to a bi-cellular vortices, which occupies much of the cavity as shown in Fig. 10a(ii). This is because the buoyancy force dominates the forced flow in the cavity. As Ri increases to 5.0, the bi-cellular vortices merge into a single vortex and become slightly large as presented in Fig. 10a(iii). Further increase of Ri at 10.0, the patterns of the streamlines are about the same as those for $Ri = 5.0$, but, a careful observation indicates that the inner vortex become larger slightly in size and stronger in strength compared this with the upper one, because the effect of free convection on heat transfer and flow increases with increasing Ri. From Figs. 10b(i)–(iv) it has been seen that the isothermal lines are nearly parallel to the vertical heated wall for $Ri = 0.0$, this indicating a dominant heat conduction mechanism. For the larger Ri ($Ri = 2.5, 5.0, 10.0$) the high temperature region become more concentrated and thin near the hot wall, and the other isothermal lines uniformly distributed in the remaining parts of the cavity.

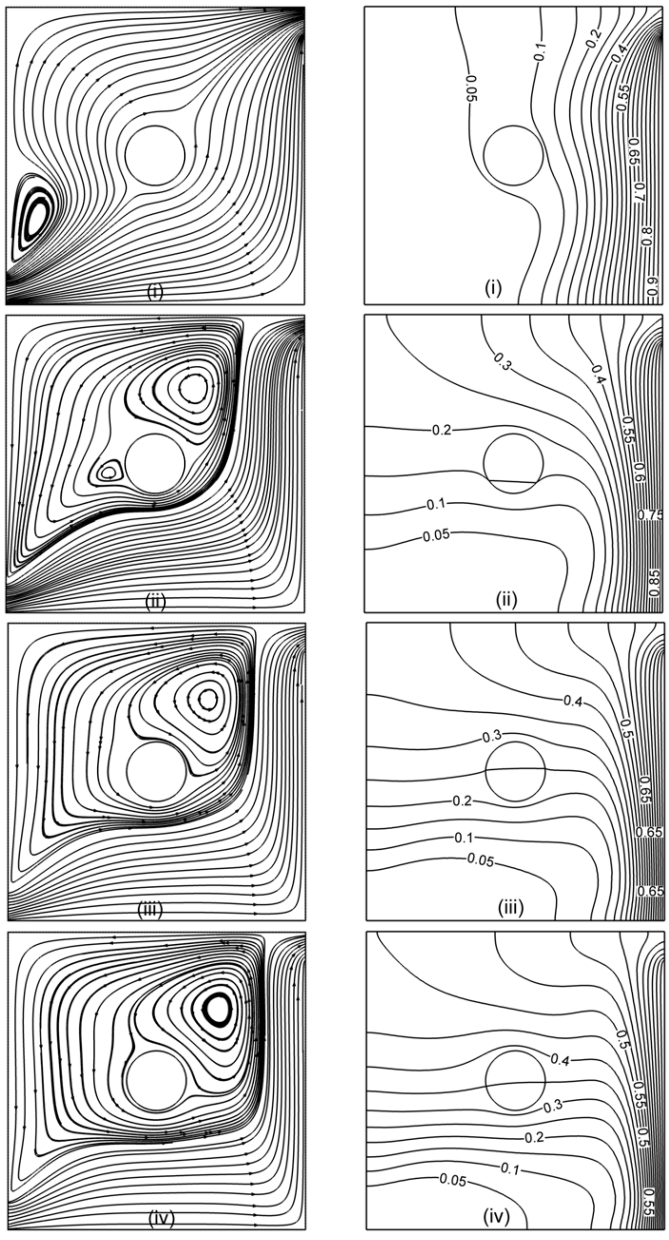

Fig. 10. (a) Streamlines and (b) isotherms for the BT configuration at (i) $Ri = 0.0$, $Ri = 2.5$, (iii) $Ri = 5.0$ and (iv) $Ri = 10.0$, while $AR = 1.0$, $Re = 100$, $K = 5.0$, $D = 0.2$, $L_x = L_y = 0.5$ and $Pr = 0.71$.

5.6 Effect of Prandtl number

The influence of Prandtl number on streamlines as well as isotherms for the BT configuration at $AR = 1.0$, $Re = 100$, $Ri = 1.0$, $D = 0.2$, $L_x = L_y = 0.5$ and $K = 5.0$ has been demonstrated in Fig. 11. The flow with small Prandtl number ($Pr = 0.71$) has been affected by the buoyancy force, thus creating a CCW recirculation region near the left top corner in the cavity as shown in Fig. 11a(i). This recirculation region decreases with increasing Prandtl numbers as shown in Figs. 11a(ii)–(iv). The isotherms illustrate the temperature field in the separated flow region has been shown in Fig. 11b(i)–(iv). The last line from the heated wall is the line with $\theta_1 = 0.05$ for all the Prandtl numbers presented in this figure. The most significant information in these plots is the shifting of the θ_1 line for the different Prandtl numbers. For the case of $Pr = 0.71$ this line moves under the cylinder placed at the center in the cavity. With increasing Prandtl numbers, that line moves towards the heated wall. The area enclosed between the θ_1 line and the heated wall can be considered as the thermally influenced region of the fluid by the heated wall. The large region that is associated with a smaller Prandtl number indicates the relatively strong thermal conduction component in these fluids.

The variation of average Nusselt number (Nu) at the heated wall and average temperature of the fluid in the cavity along with Richardson number for different Prandtl numbers has been presented in Fig. 13. From this figure it is clearly seen that for a particular values of Ri the average Nusselt number is the highest and average temperature is the lowest for the large Prandtl number $Pr = 7.1$. This is because, the fluid with the highest Prandtl number is capable to carried more heat away from the heat source and dissipated through the out flow opening in the cavity.

5.7 Effect of cylinder locations

The effect of the cylinder location on the thermal transport has great importance and has been shown in Figs. 12 and 14. Streamlines and isothermal lines for various cylinder locations have been shown in Fig. 12 for $AR = 1.0$, $Re = 100$, $Ri = 1.0$, $D = 0.2$, $Pr = 0.71$ and $K = 5.0$. As the cylinder moves closer to the left insulated wall along the mid-horizontal plane and closer to the top insulated wall along the mid-vertical plane, a large circulation cell with inner vortex has confined at the left top portion in the cavity as shown in Figs. 12a(i) and 12a(iv) respectively, and concentrated thermal layer has developed around the heat source as shown in Figs. 12b(i) and 12b(iv) respectively. Further, if the cylinder moves near the heat source along the mid-horizontal plane, the recirculating cell reduces as shown in Fig. 12a(ii) and concentrated isotherms become vertical at the heat source. However, the size of the recirculating cell reduces dramatically if the solid body is located lower in the cavity as shown in Fig. 12a(iii) and the isothermal lines are more vertically concentrated around the heat source as exposed in Fig. 12b(iii), which is similar to conduction-like mechanism.

The average Nusselt numbers at the heated surface and the average temperatures in the cavity are plotted against Richardson numbers for four different cylinder locations have been shown in Fig. 14. From this figure it is seen that the Nu is the highest when the cylinder moves closer to the left insulated wall along the mid-horizontal plane and closer

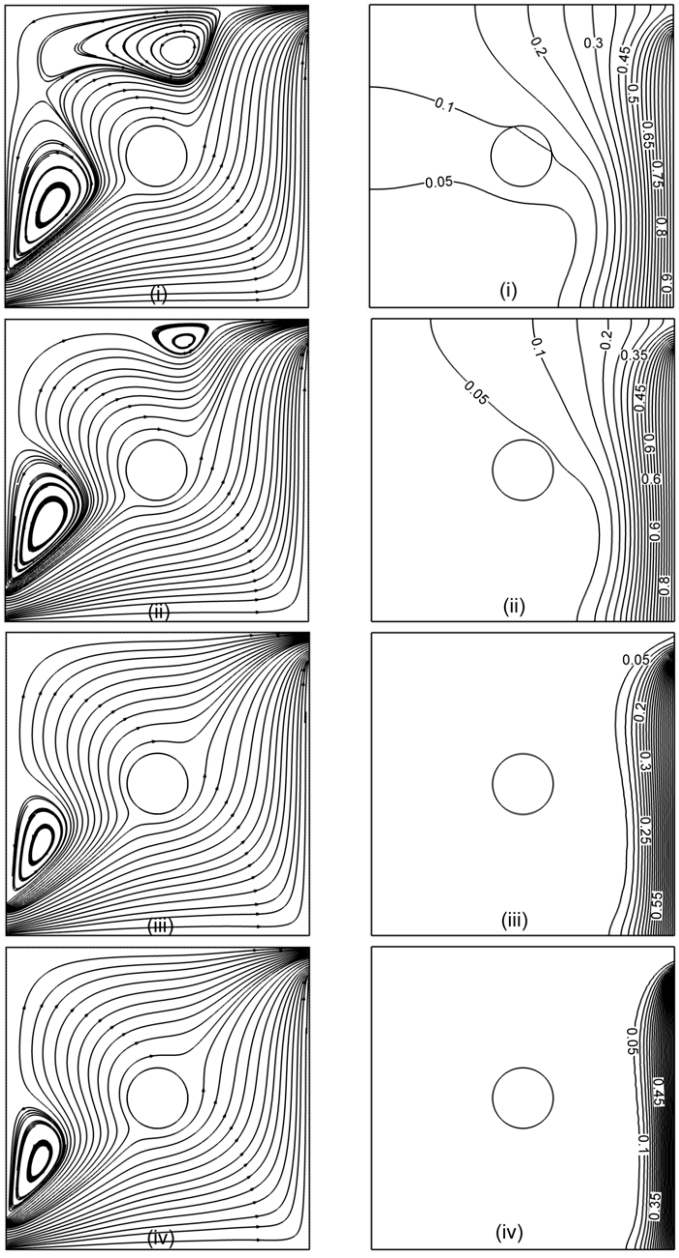

Fig. 11. (a) Streamlines and (b) isotherms for the BT configuration at (i) $Pr = 0.71$, (ii) $Pr = 1.0$, (iii) $Pr = 3.0$ and (iv) $Pr = 7.1$, while $AR = 1.0$, $Re = 100$, $Ri = 1.0$, $K = 5.0$, $L_x = L_y = 0.5$ and $D = 0.2$.

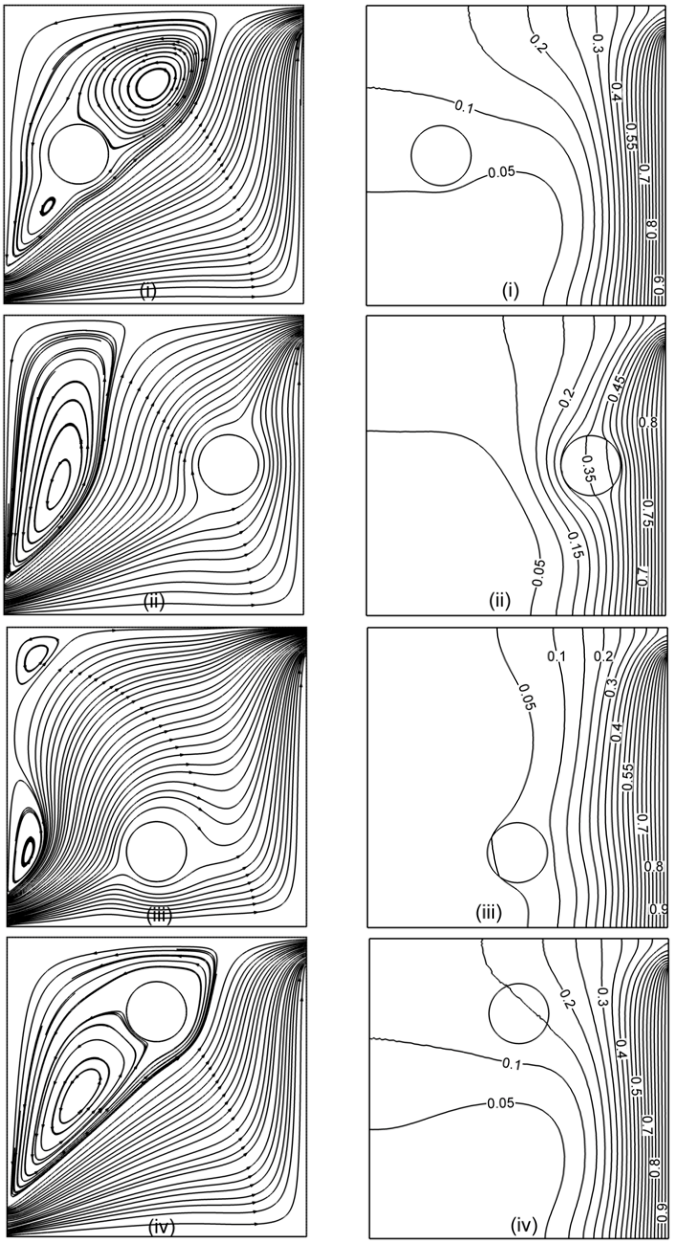

Fig. 12. (a) Streamlines and (b) isotherms for the BT configuration at (i) $L_x = 0.25$, $L_y = 0.5$, (ii) $L_x = 0.75$, $L_y = 0.5$, (iii) $L_x = 0.5$, $L_y = 0.25$ and (iv) $L_x = 0.5$, $L_y = 0.75$, while $AR = 1.0$, $Re = 100$, $Ri = 1.0$, $K = 5.0$, $D = 0.2$ and $Pr = 0.71$.

to the top insulated wall along the mid-vertical plane up to $Ri = 4.0$, beyond this the value of Ri, Nu is the highest when the cylinder moves near the heat source along the mid-horizontal plane. The average temperature of the fluid in the cavity is the lowest when the cylinder moves closer to the left insulated wall along the mid-horizontal plane and closer to the top insulated wall along the mid-vertical plane for $Ri \leq 0.5$, beyond this value of Ri, Nu is the lowest when the cylinder moves closer to the bottom insulated wall along the mid-vertical plane as Ri increases.

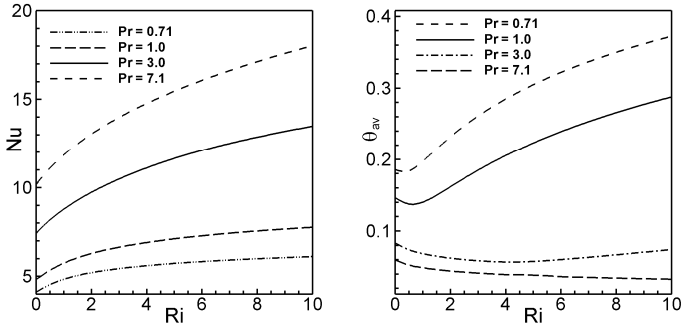

Fig. 13. Effect of Prandtl number on average Nusselt number and average temperature for the BT configuration while $AR = 1.0$, $Re = 100$, $D = 0.2$, $L_x = L_y = 0.5$ and $K = 5.0$.

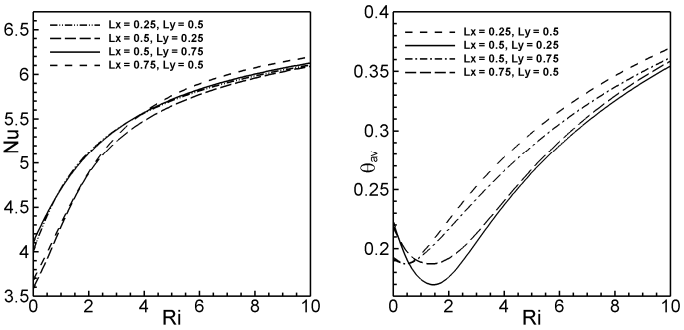

Fig. 14. Effect of cylinder locations on average Nusselt number and average temperature for the BT configuration while $AR = 1.0$, $Re = 100$, $Pr = 0.71$, $D = 0.2$ and $K = 5.0$.

5.8 Effect of cavity aspect ratio

The results presented in the preceding are for a square cavity for which the aspect ratio AR is 1. In order to investigate the convective heat transfer behavior at other aspect ratios, computations have also been done for the BT configuration at three additional aspect ratios of $0.5, 1.5$ and 2.0, while keeping $Re = 100$, $Ri = 1.0$, $Pr = 0.71$, $K = 5.0$, $L_x = L_y = 0.5$ and $D = 0.2$. The flow patterns and temperature fields for $AR = 0.5, 1.0, 1.5$, and 2.0 have been compared in Figs. 15, 16.

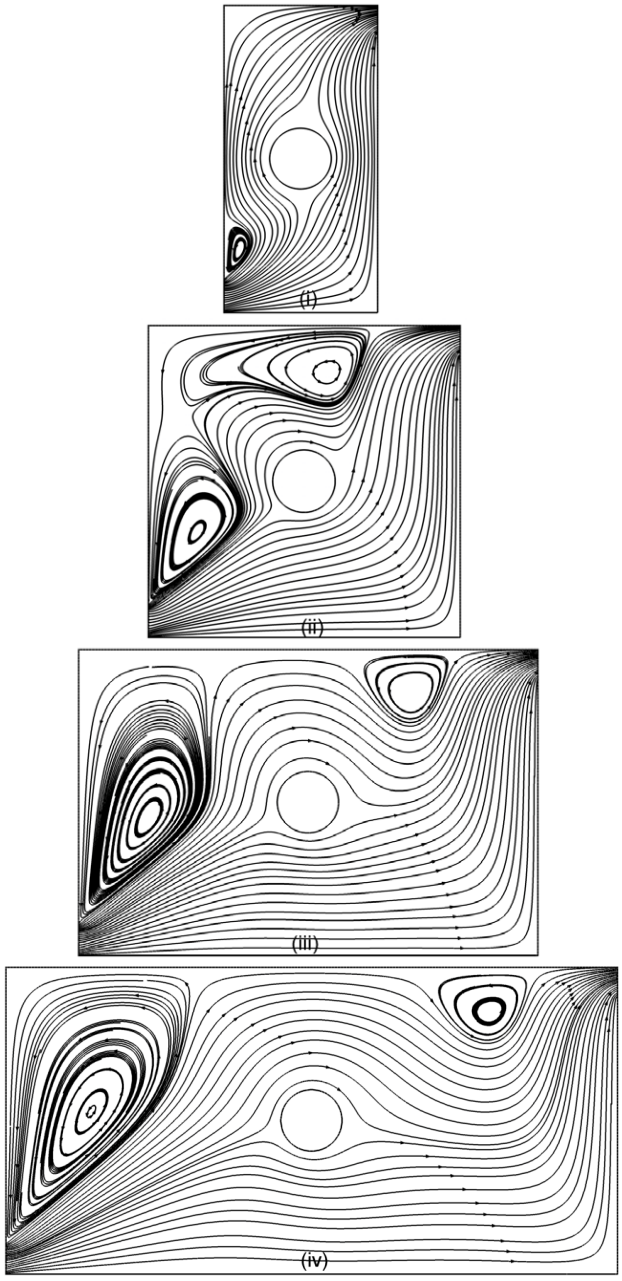

Fig. 15. Streamlines for the BT configuration at (i) $AR = 0.5$, (ii) $AR = 1.0$, (iii) $AR = 1.5$ and (iv) $AR = 2.0$, while $Re = 100$, $K = 5.0$, $Ri = 1.0$, $L_x = L_y = 0.5$, $D = 0.2$ and $Pr = 0.71$.

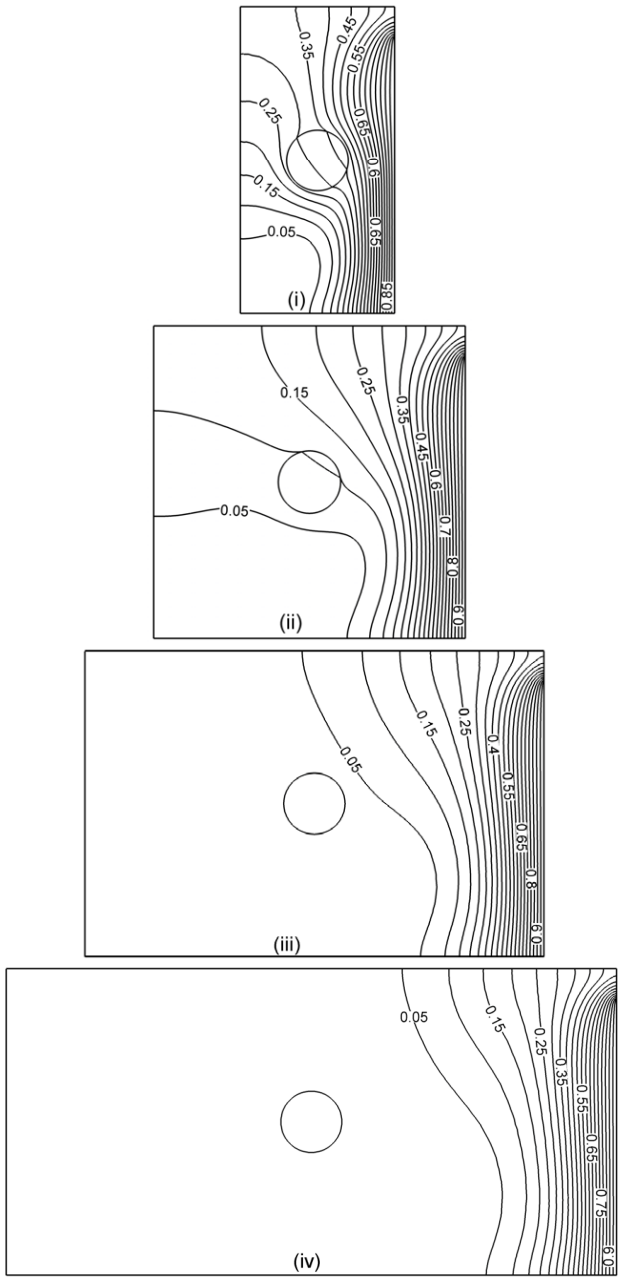

Fig. 16. Isotherms for the BT configuration at (i) $AR = 0.5$, (ii) $AR = 1.0$, (iii) $AR = 1.5$ and (iv) $AR = 2.0$, while $Re = 100$, $K = 5.0$, $Ri = 1.0$, $D = 0.2$, $L_x = L_y = 0.5$ and $Pr = 0.71$.

From Figs. 15(i)–(iv), it has been seen that for $AR = 0.5$ a small recirculation cell has developed just above the inlet position. This recirculation cell gradually increases with the increase of the value of AR, due to increasing the available space for the fluid in the cavity. On the other hand, another recirculation cell of the same size has also been located near the top surface for $AR = 1.0$ and it is reduces in size and the cell near the let wall become increases in size for $AR = 1.5$ and 2.0. Isotherms for these cases have been shown in Figs. 16(i)–(iv). It has been seen from these figures that the isothermal lines are nonlinear and occupy most of the part of the cavity for the case of $AR = 0.5$, the isothermal lines becomes linear and concentrated near the hot wall in the cavity with the increasing values of AR, because of the distance between the hot wall and the inlet, through which fresh cold fluid enter in the cavity.

The average Nusselt number (Nu) at the heat source and the average temperature of the fluid in the cavity for $AR = 0.5, 1.0, 1.5$ and 2.0 have been shown in Fig. 17. It has been seen that for a particular value of Ri the average Nusselt number at the hot wall and the average temperature of the fluid in the cavity decrease with increasing values of AR. This is because the increasing value of AR increases the available space for the fluid in the cavity.

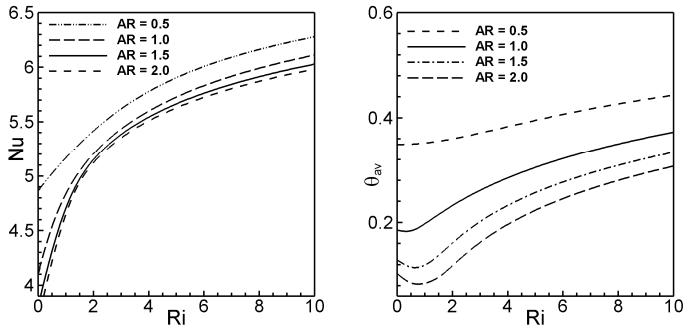

Fig. 17. Effect of cavity aspect ratio on average Nusselt number and average temperature for the BT configuration at while $Re = 100$, $Pr = 0.71$, $D = 0.2$, $L_x = L_y = 0.5$ and $K = 5.0$.

6 Conclusion

A finite element method for steady-state incompressible conjugate effect of mixed convection and conduction has been presented. The finite element equations have been derived from the governing equations that consist of the conservation of mass, momentum and energy equations. The derived finite element equations are nonlinear requiring an iterative technique solver. The Newton-Raphson iteration method has been applied to solve these nonlinear equations for solutions of the nodal velocity components, temperatures and pressures. The present study demonstrates the capability of the finite element formulation

that can provide insight to steady-state incompressible conjugate effect of mixed convection and conduction problem.

The qualitative and quantitative understanding of the influences of conjugate conduction-convection heat exchange has also been presented in this study. Attention is focused on identifying the optimum placement of inlet and outlet port for the best cooling effectiveness and on the effects of the Reynolds number, Richardson number, Prandtl number, cylinder diameter, solid-fluid thermal conductivity ratio, location of the cylinder in the cavity and the aspect ratio of the cavity. The major results have been drawn as follows:

- Cavity orientation has a great influence on the streamlines and isotherms distributions. Comparatively large buoyancy induced vortex is located for BB configuration and relatively small buoyancy induced vortex is located for TT configuration. The thermal influenced region is comparatively bulky for BB configuration and slim for TT configuration. The average Nusselt number at the hot wall has been used to compare the heat transfer rate among different configurations. Results show that the configuration BT has the highest heat transfer rates, whereas configuration BB has the lowest effective heat transfer rate.

- Diameter of cylinder affects strongly the streamline distribution in the cavity. As a result, buoyancy-induced circulation cell reduces with increasing cylinder diameter. Comparatively small effect on the isotherms is observed for different cylinder diameter. The highest heat transfer is observed for the large cylinder diameter $D = 0.4$ at $Ri \leq 5.0$, but after this the cylinder diameters have negligible effect on the heat transfer.

- Material properties (K) have insignificant effect on the flow field and have significant effect on the thermal fields. An unexpected result is found for the dependence of thermal transport on the ratio (K) of the thermal conductivity of the solid cylinder to that of the fluid. Negligibly small effect on the thermal phenomenon is observed for small cylinder size. But for large cylinder size, the variation of average Nusselt number at the hot wall is significantly influenced by the ratio K. Enhancement in the heat transfer is observed for the lowest thermal conductivity ratio.

- The forced convection parameter Re has a significant effect on the flow and temperature fields. Buoyancy-induced vortex in the streamlines increased and thermal layer near the heated surface become thin and concentrated with increasing values of Re. The average Nusselt numbers at the heated surface is always the highest and the average temperature of the fluid in the cavity is the lowest for the large value of Re.

- Mixed convection parameter Ri affects strongly on the flow and temperature fields. The recirculation cell due to heat source in the streamlines plot become large and the concentrated thermal layer near the heated surface become thin with increasing Ri.

- The influence of Prandtl number on streamlines and isotherms are remarkable for the different values of Pr. Increasing the Prandtl number increase the average Nusselt number at the hot wall and decrease the average temperature of the fluid in the cavity.

- Locations of the cylinder have significant effect on the flow and thermal fields. The value of average Nusselt number (Nu) at the hot wall and the average temperature of the fluid in the cavity vary non-monotonically with the cylinder location in the cavity.
- The cavity aspect ratio has significant effect on the flow and temperature fields. The buoyancy induced recirculation cell increase and the heat transfer become conduction dominated with increasing the cavity aspect ratio. The average Nusselt number at the hot wall is always the highest for $AR = 0.5$ and the average temperature of the fluid in the cavity is the lowest for $AR = 2.0$.

Acknowledgements

The authors like to express their gratitude to the Department of Mathematics, Bangladesh University of Engineering and Technology, for providing computer facility during this work.

Appendix

Finite element formulation

To derive the finite element equations, the method of weighted residuals (Zienkiewicz [14]) is applied to the equations (1)–(5) as

$$\int_A N_\alpha \left(\frac{\partial U}{\partial X} + \frac{\partial U}{\partial Y} \right) \mathrm{d}A = 0, \tag{A.1}$$

$$\int_A N_\alpha \left(U\frac{\partial U}{\partial X} + V\frac{\partial U}{\partial Y} \right) \mathrm{d}A = -\int_A H_\lambda \left(\frac{\partial P}{\partial X} \right) \mathrm{d}A + \frac{1}{Re}\int_A N_\alpha \left(\frac{\partial^2 U}{\partial X^2} + \frac{\partial^2 U}{\partial Y^2} \right) \mathrm{d}A, \tag{A.2}$$

$$\int_A N_\alpha \left(U\frac{\partial V}{\partial X} + V\frac{\partial V}{\partial Y} \right) \mathrm{d}A = -\int_A H_\lambda \left(\frac{\partial P}{\partial Y} \right) \mathrm{d}A + \frac{1}{Re}\int_A N_\alpha \left(\frac{\partial^2 V}{\partial X^2} + \frac{\partial^2 V}{\partial Y^2} \right) \mathrm{d}A + Ri\int_A N_\alpha \theta \, \mathrm{d}A, \tag{A.3}$$

$$\int_A N_\alpha \left(U\frac{\partial \theta}{\partial X} + V\frac{\partial \theta}{\partial Y} \right) \mathrm{d}A = \frac{1}{Re\,Pr}\int_A N_\alpha \left(\frac{\partial^2 \theta}{\partial X^2} + \frac{\partial^2 \theta}{\partial Y^2} \right) \mathrm{d}A, \tag{A.4}$$

$$0 = \int_A N_\alpha \left(\frac{\partial^2 \theta}{\partial X^2} + \frac{\partial^2 \theta}{\partial Y^2} \right) \mathrm{d}A, \tag{A.5}$$

where A is the element area, N_α ($\alpha = 1, 2, \ldots, 6$) are the element interpolation functions for the velocity components and the temperature, and H_λ ($\lambda = 1, 2, 3$) are the element interpolation functions for the pressure.

Gauss's theorem is then applied to equations (A.2)–(A.5) to generate the boundary integral terms associated with the surface tractions and heat flux. Then equations (A.2)–(A.5) becomes,

$$\int_A N_\alpha \left(U\frac{\partial U}{\partial X} + V\frac{\partial U}{\partial Y} \right) \mathrm{d}A + \int_A H_\lambda \left(\frac{\partial P}{\partial X} \right) \mathrm{d}A + \frac{1}{Re}\int_A \left(\frac{\partial N_\alpha}{\partial X}\frac{\partial U}{\partial X} + \frac{\partial N_\alpha}{\partial Y}\frac{\partial U}{\partial Y} \right) \mathrm{d}A = \int_{S_0} N_\alpha S_x \, \mathrm{d}S_0, \tag{A.6}$$

$$\int_A N_\alpha \left(U\frac{\partial V}{\partial X} + V\frac{\partial V}{\partial Y} \right) \mathrm{d}A + \int_A H_\lambda \left(\frac{\partial P}{\partial Y} \right) \mathrm{d}A + \frac{1}{Re}\int_A \left(\frac{\partial N_\alpha}{\partial X}\frac{\partial V}{\partial X} + \frac{\partial N_\alpha}{\partial Y}\frac{\partial V}{\partial Y} \right) \mathrm{d}A - Ri\int_A N_\alpha \theta \, \mathrm{d}A = \int_{S_0} N_\alpha S_y \, \mathrm{d}S_0, \tag{A.7}$$

$$\int_A N_\alpha \left(U\frac{\partial \theta}{\partial X} + V\frac{\partial \theta}{\partial Y} \right) \mathrm{d}A + \frac{1}{Re\,Pr}\int_A \left(\frac{\partial N_\alpha}{\partial X}\frac{\partial \theta}{\partial X} + \frac{\partial N_\alpha}{\partial Y}\frac{\partial \theta}{\partial Y} \right) \mathrm{d}A = \int_{S_w} N_\alpha q_{1w} \, \mathrm{d}S_w, \tag{A.8}$$

$$\int_A \left(\frac{\partial N_\alpha}{\partial X}\frac{\partial \theta}{\partial X} + \frac{\partial N_\alpha}{\partial Y}\frac{\partial \theta}{\partial Y} \right) \mathrm{d}A = \int_{S_w} N_\alpha q_{2w} \, \mathrm{d}S_w. \tag{A.9}$$

Here (A.6), (A.7) specifying surface tractions (S_x, S_y) along outflow boundary S_0 and (A.8), (A.9) specifying velocity components and fluid temperature or heat flux (q_w) that flows into or out from domain along wall boundary S_w.

The basic unknowns for the above differential equations are the velocity components, U, V, the temperature, θ, and the pressure P. The six node triangular element is used in this work for the development of the finite element equations. All six nodes are associated with velocities as well as temperature; only the corner nodes are associated with pressure. This means that a lower order polynomial is chosen for pressure. The element assumes quadratic interpolation for the velocity component and the temperature distributions and linear interpolation for the pressure distribution according to their highest derivative orders in the differential equations (A.1) and (A.6)–(A.9) as

$$U(X, Y) = N_\beta U_\beta, \tag{A.10}$$

$$V(X, Y) = N_\beta V_\beta, \tag{A.11}$$

$$\theta(X, Y) = N_\beta \theta_\beta, \tag{A.12}$$

$$\theta_s(X,Y) = N_\beta \theta_{s\beta}, \tag{A.13}$$

$$P(X,Y) = H_\lambda P_\lambda, \tag{A.14}$$

where $\beta = 1, 2, \ldots, 6$; $\lambda = 1, 2, 3$.

Substituting the element velocity component distributions, the temperature distribution, and the pressure distribution from equations (A.10)–(A.14), the finite element equations can be written in the form,

$$K_{\alpha\beta^x} U_\beta + K_{\alpha\beta^y} V_\beta = 0, \tag{A.15}$$

$$K_{\alpha\beta\gamma^x} U_\beta U_\gamma + K_{\alpha\beta\gamma^y} V_\gamma U_\gamma + M_{\alpha\mu^x} P_\mu + \frac{1}{Re}(S_{\alpha\beta^{xx}} + S_{\alpha\beta^{yy}}) U_\beta = Q_{\alpha^U}, \tag{A.16}$$

$$K_{\alpha\beta\gamma^x} U_\beta V_\gamma + K_{\alpha\beta\gamma^y} V_\gamma V_\gamma + M_{\alpha\mu^y} P_\mu + \frac{1}{Re}(S_{\alpha\beta^{xx}} + S_{\alpha\beta^{yy}}) V_\beta - Ri\, K_{\alpha\beta}\theta_\beta = Q_{\alpha^V}, \tag{A.17}$$

$$K_{\alpha\beta\gamma^x} U_\beta \theta_\gamma + K_{\alpha\beta\gamma^y} V_\beta \theta_\gamma + \frac{1}{Re\, Pr}(S_{\alpha\beta^{xx}} + S_{\alpha\beta^{yy}})\theta_\beta = Q_{\alpha^\theta}, \tag{A.18}$$

$$(S_{\alpha\beta^{xx}} + S_{\alpha\beta^{yy}})\theta_\beta = Q_{\alpha^{\theta_s}}, \tag{A.19}$$

where the coefficients in element matrices are in the form of the integrals over the element area and along the element edges S_0 and S_w as,

$$K_{\alpha\beta^x} = \int_A N_\alpha N_{\beta,x}\, \mathrm{d}A, \tag{A.20a}$$

$$K_{\alpha\beta^y} = \int_A N_\alpha N_{\beta,y}\, \mathrm{d}A, \tag{A.20b}$$

$$K_{\alpha\beta\gamma^x} = \int_A N_\alpha N_\beta N_{\gamma,x}\, \mathrm{d}A, \tag{A.20c}$$

$$K_{\alpha\beta\gamma^y} = \int_A N_\alpha N_\beta N_{\gamma,y}\, \mathrm{d}A, \tag{A.20d}$$

$$K_{\alpha\beta} = \int_A N_\alpha N_\beta\, \mathrm{d}A, \tag{A.20e}$$

$$S_{\alpha\beta^{xx}} = \int_A N_{\alpha,x} N_{\beta,x}\, \mathrm{d}A, \tag{A.20f}$$

$$S_{\alpha\beta^{yy}} = \int_A N_{\alpha,y} N_{\beta,y}\, \mathrm{d}A, \tag{A.20g}$$

$$M_{\alpha\mu^x} = \int_A H_\alpha H_{\mu,x}\, \mathrm{d}A, \tag{A.20h}$$

$$M_{\alpha\mu^y} = \int_A N_\alpha H_{\mu,y}\, \mathrm{d}A, \tag{A.20i}$$

$$Q_{\alpha^U} = \int_{S_0} N_\alpha S_x \, \mathrm{d}S_0, \tag{A.20j}$$

$$Q_{\alpha^V} = \int_{S_0} N_\alpha S_y \, \mathrm{d}S_0, \tag{A.20k}$$

$$Q_{\alpha^\theta} = \int_{S_w} N_\alpha q_{1w} \, \mathrm{d}S_w, \tag{A.20l}$$

$$Q_{\alpha^{\theta_s}} = \int_{S_w} N_\alpha q_{2w} \, \mathrm{d}S_w, \tag{A.20m}$$

These element matrices are evaluated in closed-form ready for numerical simulation. Details of the derivation for these element matrices are omitted herein for brevity.

Computational procedure

The derived finite element equations, equations (A.15)–(A.19), are nonlinear. These nonlinear algebraic equations are solved by applying the Newton-Raphson iteration technique by first writing the unbalanced values from the set of the finite element equations (A.15)–(A.19) as,

$$F_{\alpha^p} = K_{\alpha\beta^x} U_\beta + K_{\alpha\beta^y} V_\beta, \tag{A.21a}$$

$$F_{\alpha^U} = K_{\alpha\beta\gamma^x} U_\beta U_\gamma + K_{\alpha\beta\gamma^y} V_\beta U_\gamma + M_{\alpha\mu^x} P_\mu + \frac{1}{Re}(S_{\alpha\beta^{xx}} + S_{\alpha\beta^{yy}}) U_\beta - Q_{\alpha^U}, \tag{A.21b}$$

$$F_{\alpha^V} = K_{\alpha\beta\gamma^x} U_\beta V_\gamma + K_{\alpha\beta\gamma^y} V_\gamma V_\gamma + M_{\alpha\mu^y} P_\mu + \frac{1}{Re}(S_{\alpha\beta^{xx}} + S_{\alpha\beta^{yy}}) V_\beta - Ri\, K_{\alpha\beta}\theta_\beta - Q_{\alpha^V}, \tag{A.21c}$$

$$F_{\alpha^\theta} = K_{\alpha\beta\gamma^x} U_\beta \theta_\gamma + K_{\alpha\beta\gamma^y} V_\beta \theta_\gamma + \frac{1}{Re\, Pr}(S_{\alpha\beta^{xx}} + S_{\alpha\beta^{yy}})\theta_\beta - Q_{\alpha^\theta}, \tag{A.21d}$$

$$F_{\alpha^{\theta_s}} = (S_{\alpha\beta^{xx}} + S_{\alpha\beta^{yy}})\theta_\beta - Q_{\alpha^{\theta_s}}. \tag{A.21e}$$

This leads to a set of algebraic equations with the incremental unknowns of the element nodal velocity components, temperatures, and pressures in the form,

$$\begin{bmatrix} K_{PU} & K_{PV} & 0 & 0 & 0 \\ K_{UU} & K_{UV} & 0 & K_{UP} & 0 \\ K_{\theta U} & K_{\theta V} & K_{\theta\theta} & 0 & 0 \\ K_{VU} & K_{VV} & K_{V\theta} & K_{VP} & 0 \\ 0 & 0 & 0 & 0 & K_{\theta_s\theta_s} \end{bmatrix} \begin{Bmatrix} \Delta P \\ \Delta U \\ \Delta\theta \\ \Delta V \\ \Delta\theta_s \end{Bmatrix} = - \begin{Bmatrix} F_{\alpha^P} \\ F_{\alpha^U} \\ F_{\alpha^\theta} \\ F_{\alpha^V} \\ F_{\alpha^{\theta_s}} \end{Bmatrix}, \tag{A.22}$$

where

$$K_{UU} = K_{\alpha\beta\gamma^x} U_\beta + K_{\alpha\beta\gamma^y} U_\gamma + K_{\alpha\beta\gamma^y} V_\beta + \frac{1}{Re}(S_{\alpha\beta^{xx}} + S_{\alpha\beta^{yy}}),$$

$$
\begin{aligned}
K_{VV} &= K_{\alpha\beta\gamma^x}U_\beta + K_{\alpha\beta\gamma^y}V_\gamma + K_{\alpha\beta\gamma^y}V_\gamma + \frac{1}{Re}(S_{\alpha\beta^{xx}} + S_{\alpha\beta^{yy}}),\\
K_{\theta\theta} &= K_{\alpha\beta\gamma^x}U_\beta + K_{\alpha\beta\gamma^y}V_\beta + \frac{1}{Re\,Pr}(S_{\alpha\beta^{xx}} + S_{\alpha\beta^{yy}}),\\
K_{\theta_s\theta_s} &= S_{\alpha\beta^{xx}} + S_{\alpha\beta^{yy}},\\
K_{UV} &= K_{\alpha\beta\gamma^y}U_\gamma, \quad K_{VU} = K_{\alpha\beta\gamma^x}V_\gamma, \quad K_{\theta U} = K_{\alpha\beta\gamma^x}\theta_\gamma,\\
K_{\theta V} &= K_{\alpha\beta\gamma^y}\theta_\gamma, \quad K_{PU} = K_{\alpha\beta\gamma^x}, \quad K_{PV} = K_{\alpha\beta\gamma^y},\\
K_{UP} &= K_{\alpha\mu^x}, \quad K_{VP} = K_{\alpha\mu^y}, \quad K_{V\theta} = -Ri\,K_{\alpha\beta},\\
K_{U\theta} &= K_{U\theta_s} = K_{V\theta_s} = K_{\theta P} = K_{\theta\theta_s} = K_{PP} = K_{P\theta} = K_{P\theta_s} = 0,\\
K_{\theta_s U} &= K_{\theta_s V} = K_{\theta_s\theta} = K_{\theta_s P} = 0.
\end{aligned}
$$

The iteration process is terminated if the percentage of the overall change compared to the previous iteration is less than the specified value.

To solve the sets of the global nonlinear algebraic equations in the form of matrix, the Newton-Raphson iteration technique has been adapted through PDE solver with MATLAB interface. The convergence of solutions is assumed when the relative error for each variable between consecutive iterations is recorded below the convergence criterion ε such that $|\Psi^{m+1} - \Psi^m| \leq 10^{-4}$, where n is number of iteration and $\Psi = U, V, \theta$.

References

1. A. Omri, S. B. Nasrallah, Control volume finite element numerical simulation of mixed convection in an air-cooled cavity, *Numerical Heat Tr. A-Appl.*, **36**, pp. 615–637, 1999.
2. S. Singh, M. A. R. Sharif, Mixed convection cooling of a rectangular cavity with inlet and exit openings on differentially heated side walls, *Numerical Heat Tr. A-Appl.*, **44**, pp. 233–253, 20003.
3. O. Manca, S. Nardini, K. Khanafer, K. Vafai, Effect of heated wall position on mixed convection in a channel with an open cavity, *Numerical Heat Tr. A-Appl.*, **43**, pp. 259–282, 2003.
4. O. Manca, S. Nardini, K. Vafai, Experimental investigation of mixed convection in a channel with an open cavity, *Exp. Heat Transfer*, **19**, pp. 53–68, 2006.
5. O. Manca, S. Nardini, K. Vafai, Experimental analysis of opposing flow in mixed convection in a channel with an open cavity below, *Exp. Heat Transfer*, **21**, pp. 99–114, 2008.
6. M. M. Rahman, M. A. Alim, M. A. H. Mamun, M. K. Chowdhury, A. K. M. S. Islam, Numerical study of opposing mixed convection in a vented enclosure, *J. Eng. Appl. Sci.*, **2**(2), pp. 25–36, 2007.
7. S. Z. Shuja, B. S. Yilbas, M. O. Iqbal, Mixed convection in a square cavity due to heat generating rectangular body effect of cavity exit port locations, *Int. J. of Numerical Methods for Heat and Fluid Flow*, **10**(8), pp. 824–841, 2000.
8. E. Papanicolaou, Y. Jaluria, Mixed convection from an isolated heat source in a rectangular enclosure, *Numerical Heat Tr. A-Appl.*, **18**, pp. 427–461, 1990.

9. E. Papanicolaou, Y. Jaluria, Mixed convection from a localized heat source in a cavity with conducting walls, a numerical study, *Numerical Heat Tr. A-Appl.*, **23**, pp. 463–484, 1993.

10. T. H. Hsu, P. T. Hsu, S. P. How, Mixed convection in a partially divided rectangular enclosure, *Numerical Heat Tr. A-Appl.*, **31**, pp. 655–683, 1997.

11. J. R. Lee, M. Y. Ha, S. Balachandar, H. S. Yoon, S. S. Lee, Natural convection in a horizontal layer of fluid with a periodic array of square cylinders in the interior, *Phys. Fluids*, **16**, pp. 1097–1117, 2004.

12. M. Y. Ha, H. S. Yoon, K. S. Yoon, S. Balachandar, I. Kim, J. R. Lee, H. H. Chun, Two-dimensional and unsteady natural convection in a horizontal enclosure with a square body, *Numerical Heat Tr. A-Appl.*, **41**, pp. 183–210, 2002.

13. J. M. House, C. Beckermann, T. F. Smith, Effect of a centered conducting body on natural convection heat transfer in an enclosure, *Numerical Heat Tr. A-Appl.*, **18**, pp. 213–225, 1990.

14. O. C. Zienkiewicz, R. L. Taylor, *The finite element method*, 4th ed., McGraw-Hill, 1991.